Preprints of the 21st IFAC World Congress (Virtual)
Berlin, Germany, July 12-17, 2020

Motion Control of Mechanical Systems with a Cable Contacting the Ground

Maria Mikami*, Takeshi Yamamoto*, Yoshiki Sugawara, Masakazu Takeda****

* *Course of Mechanical Engineering, Graduate School of Science and Engineering, Aoyama Gakuin University, 5-10-1, Fuchinobe, Chuo-ku, Sagamihara-shi, Kanagawa-ken, Japan*
(*e-mail: c5619130@aoyama.jp; c5617126@aoyama.jp*).
***Department of Mechanical Engineering, College of Science and Engineering, Aoyama Gakuin University, 5-10-1, Fuchinobe, Chuo-ku, Sagamihara-shi, Kanagawa-ken, Japan*
(*e-mail: sugawara@me.aoyama.ac.jp; takeda@me.aoyama.ac.jp*).

Abstract: The usage of unmanned aerial vehicles (UAVs) varies from construction inspection to disaster response. Cable attachment benefits the UAV with longer operation time and larger data transmission, while the tension, inertia, and contact forces of the cable work to disturb its operation. This paper introduces a numerical modelling method of a cable with frictional contact forces using an absolute nodal coordinate formulation (ANCF), and extracts and evaluates the influences of the cable on the mechanical system's motion. The contacting cable length, that affects frictional contact forces, is derived using a catenary curve. The numerical analysis results present errors and vibrations at the connection point of the cable and the rigid body. These are the influences when the cable contacts the ground. In this paper, the compensation system, and its validity for mitigating these influences, using an unscented Kalman filter (UKF) to estimate the state of the cable, are presented. Although there was a small error in the mechanical system's final position in relation to the target position, the numerical analysis indicated that the proposed control system stabilizes the mechanical system's motion.

Keywords: UAV, Cables, Friction, ANCF, Multibody system, Catenary curve, Compensation

1. INTRODUCTION

Many researchers and industry practitioners have proposed the use of unmanned aerial vehicles (UAVs) for construction inspection and disaster response (Ohno et al., 2016). Conventional inspection techniques of large construction sites can jeopardize human safety and require cranes to inspect complicated or difficult to reach areas (Imadu et al., 2016; Ciampa et al., 2019). The use of a UAV for construction inspection was tested; however, because battery-life lasted only 2 hours, it was difficult to complete a smooth, full inspection (Ciampa et al., 2019). In a different study related to disaster response, an aerial robot and a ground robot mapped inside a building damaged in the 2011 Tohoku earthquake. However, in this study, the robots were unable to access certain areas because physical obstacles disrupted their operations (Michael et al., 2012). Koyanagi (2016) states that radiation is another possible disturbance that affects UAV data transmission. As a result, the combination of wired and non-wired technology was the solution to this situation.

In disaster response conditions, wireless communication is not stable nor reliable (Nagatani et al., 2013), thus, communication through a cable is a realistic solution. Cable attachment benefits the UAV with longer operation time and larger transmission of data. However, the tension, inertia, and contact forces of the cable work can work to disturb the UAV's operation (Imadu et al., 2016; Yamamoto et al., 2019). The optimal cable length is reported by Imadu et al. (2016). In a different study, the linearization to simplify the control method of a UAV was examined, yet this system did not include external force fluctuations (Rubio, 2018). Further, a control method to reduce the disturbance in a quadrotor has been studied; nonetheless, a cable was not included into the control objective, which should be a nonlinear model (Rubio et al., 2019). The control system to compensate for the influences of a cable load is proposed and verified in the analysis (Yamamoto et al., 2019).

The focus of this research is the control system for when the attached cable contacts obstacles, the ground or buildings. Particularly, the contact between the two suspending points of the cable is examined.

This paper is organized as follows: The analysis model and the frictional contact forces on a cable are introduced in Section 2. The numerical analysis is presented, and the influences of the cable friction forces are evaluated in Section 3. The applied control system is explained in Section 4. The state estimation for the control system is explained in Section 5. The numerical analysis to show the validity of the proposed control system is illustrated in Section 6. Conclusions are given in Section 7.

2. ANALYSIS MODEL

This section presents the analysis model of the objective mechanical system with a cable attached. The model is composed of a rigid body and cable. Both ends of the cable are pin supported by the wall and the rigid body respectively. Here is the list of assumptions for the model:

- The diameter and density of the cable and the density of the rigid body are constant.

- The rigid body is a cube shape.
- Gravitational force is applied downwards.
- There is no air resistance.
- The contact surface is rigid and parallel to the X-axis.
- Sensors obtain the X, Y, θ of both ends of the cable, and their derivatives with respect to time.

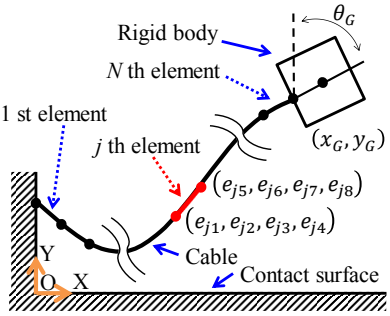

Fig. 1. Control object model.

2.1 Equation of Motion

Since the cable is flexible, Absolute Nodal Coordinate Formulation (ANCF) proposed in Berzeri et al. (2000) is employed in the cable. This formulation method is a type of a non-linear Finite Elements Method (FEM) which can express large deformation and rotation using only a few elements.

The cable is divided into N beam elements and the nodal coordinate is defined at both ends of each beam element. The nodal coordinate vector of j-th element is defined as (1), and the deformation and the gradient in the absolute coordinate system is defined as (2).

$$\mathbf{q}_{cj} = \begin{bmatrix} e_{j1} & e_{j2} & e_{j3} & e_{j4} & e_{j5} & e_{j6} & e_{j7} & e_{j8} \end{bmatrix}^T. \quad (1)$$

$$\begin{aligned} &e_{j1} = X_j\big|_{x_j=0}, e_{j2} = Y_j\big|_{x_j=0}, e_{j3} = \left.\frac{\partial X_j}{\partial x_j}\right|_{x_j=0}, e_{j4} = \left.\frac{\partial Y_j}{\partial x_j}\right|_{x_j=0}, \\ &e_{j5} = X_j\big|_{x_j=l_j}, e_{j6} = Y_j\big|_{x_j=l_j}, e_{j7} = \left.\frac{\partial X_j}{\partial x_j}\right|_{x_j=l_j}, e_{j8} = \left.\frac{\partial Y_j}{\partial x_j}\right|_{x_j=l_j}. \end{aligned} \quad (2)$$

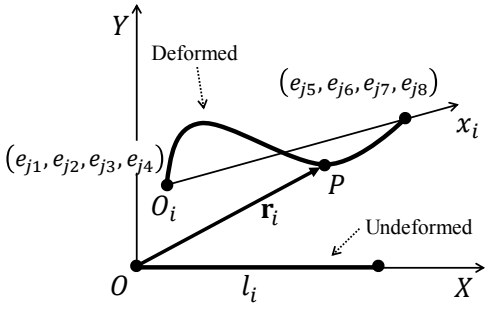

Fig. 2. The j-th cable element by ANCF.

Therefore, the global coordinate vector of an arbitrary point P on the neutral axis of j-th element is expressed as

$$\mathbf{r}_j = \mathbf{S}_j \mathbf{q}_{cj}, \quad (3)$$

where $\mathbf{S}_j$ is the interpolation function matrix. The coordinate vector is defined as (4), consists of horizontal coordinate x_G, vertical coordinate y_G, and rotational coordinate θ_G.

$$\mathbf{q}_r = \begin{bmatrix} x_G & y_G & \theta_G \end{bmatrix}^T. \quad (4)$$

Accordingly, the generalized coordinate vector is defined as

$$\mathbf{q} = \begin{bmatrix} \mathbf{q}_{c1}{}^T & \mathbf{q}_{c2}{}^T & \cdots & \mathbf{q}_{cN}{}^T & \mathbf{q}_r{}^T \end{bmatrix}^T. \quad (5)$$

The constraint conditions are defined by $\mathbf{C} = 0$, that expresses the connection of both ends of the cable and the adjacent cable elements. The Jacobian $\mathbf{C}_q$ is derived by partially differentiating the constraint equations with respect to the generalized coordinate vector $\mathbf{q}$.

The force vector $\mathbf{Q}$ is expressed by the bending stiffness vector $\mathbf{K}_t$, the longitudinal deformation stiffness vector $\mathbf{K}_\ell$, and the external force vector $\mathbf{Q}_E$ which includes the gravitational force and the friction forces.

$$\mathbf{Q} = \mathbf{Q}_E - (\mathbf{K}_t + \mathbf{K}_\ell)\mathbf{q}. \quad (6)$$

Therefore, the Differential-algebraic Equation (DAE) is derived as (7),

$$\begin{bmatrix} \mathbf{M} & \mathbf{C}_q{}^T \\ \mathbf{C}_q & \mathbf{0} \end{bmatrix} \begin{bmatrix} \ddot{\mathbf{q}} \\ \boldsymbol{\lambda} \end{bmatrix} = \begin{bmatrix} \mathbf{Q} \\ \boldsymbol{\gamma} \end{bmatrix}, \quad (7)$$

where $\mathbf{M}$ denotes the inertia matrix, $\mathbf{C}_q$ denotes Jacobian, $\boldsymbol{\lambda}$ denotes the undetermined multiplier vector, and $\boldsymbol{\gamma}$ denotes the acceleration equation.

To organize (7) with respect to independent coordinates $\mathbf{q}_{in}$, the dependent coordinates and the undetermined multiplier vector are eliminated. Hence, (7) is organized into (8).

$$\mathbf{M}_{in}\ddot{\mathbf{q}}_{in} + (\mathbf{K}_{tin} + \mathbf{K}_{\ell in})\mathbf{q}_{in} = \mathbf{Q}_{in}. \quad (8)$$

where the $\mathbf{M}_{in}$, $\mathbf{K}_{tin}$, $\mathbf{K}_{\ell in}$, $\mathbf{Q}_{in}$ denotes the inertia matrix, the bending stiffness vector, the longitudinal deformation stiffness vector, and the force vector, respectively, they are collectively expressed in the independent coordinate system.

2.2 Contact Length Model

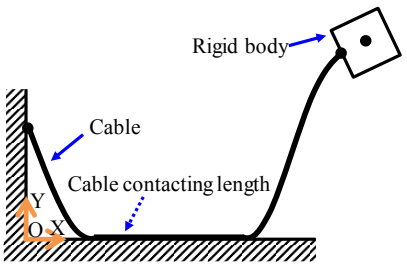

Fig. 3. The model when the cable is contacting the ground.

The frictional contact forces on the cable are introduced supposing UAVs use in rescue applications. A rescue mission to detect a person in the damaged area would have obstacles both under and above the UAV. This paper focuses on the most likely obstacle under the UAV, the ground. Frictional contact forces from the ground depends on the length of cable

contacting the surface. For simplicity, the contacting length is derived approximately from the catenary curve. Catenary value a_0 is defined by horizontal tension at the lowest point T_0, linear density w, and gravitational acceleration g as

$$a_0 = T_0 / wg. \tag{9}$$

When the catenary curve vertex is located at an arbitrary point (p, q), the catenary curve is given as

$$y = a_0\left\{\cosh\left(\frac{x-p}{a_0}\right)-1\right\}+q. \tag{10}$$

Supposing that the coordinates of the position and the angle at both ends of the cable can be obtained from the sensors, the three unknowns are derived as

$$a_0 = \frac{x_0 - x_3}{\sinh^{-1}(\tan\theta_3)-\sinh^{-1}(\tan\theta_0)}, \tag{11}$$

$$p = \frac{x_0\sinh^{-1}(\tan\theta_3)-x_3\sinh^{-1}(\tan\theta_0)}{\sinh^{-1}(\tan\theta_3)-\sinh^{-1}(\tan\theta_0)}, \tag{12}$$

$$q = y - a_0\left\{\cosh\left(\frac{x-p}{a_0}\right)-1\right\}. \tag{13}$$

The length of the catenary curve between the intersection points of the surface line and the catenary curve $(x'_1,\ x'_2)$ is approximately equal to the contacting cable length ℓ, which is expressed as

$$\ell \approx \int_{x'_1}^{x'_2}\sqrt{1+\sinh^2\left(\frac{x-p}{a_0}\right)}dx. \tag{14}$$

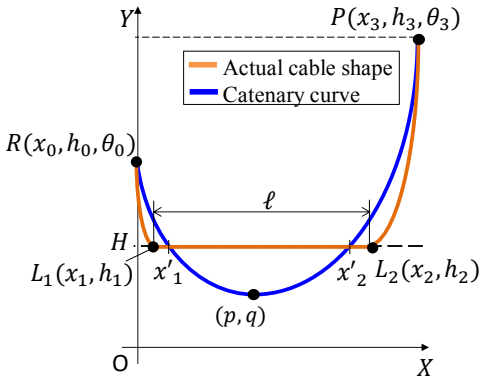

Fig. 4. Contact length model: Catenary curve and contacting cable curve.

Equation (15) is the contact force which works on each contacting cable elements, where μ is the friction coefficient.

$$\mathbf{Q}_{Ecj} = m_{cj}g\left[-\mu\ \ \frac{1}{2}\ \ 0\ \ \frac{\ell_j}{12}\ \ -\mu\ \ \frac{1}{2}\ \ 0\ \ -\frac{\ell_j}{12}\right]^T. \tag{15}$$

Friction forces are applied to the nodes that are contacting the surface. The contacting nodes are determined from the length of the non-contacting cable length. The non-contacting cable shape is approximated to be a catenary curve in which the cable inclination at the contacting point is 0. This implies the contacting point is the lowest point of the catenary curve. With the coordinates of the supporting point and the connecting point given, the catenary value for each non-contacting cable shapes are

$$a_1 = \frac{x_0 - x_1}{\sinh^{-1}(\tan\theta_0)}, \tag{16}$$

$$a_2 = \frac{x_3 - x_2}{\sinh^{-1}(\tan\theta_3)}. \tag{17}$$

Note that the contacting nodes may not match the beginning nor the end of the contacting cable.

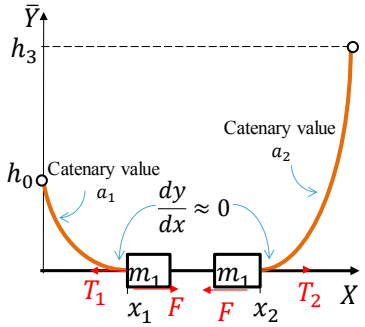

Fig. 5. Contact length model: Contacting segment model.

3. ANALYTICAL EVALUATION OF THE CABLE CONTACT FORCES: INFLUENCES ON MECHANICAL SYSTEM MOTION

This section presents the numerical analysis results of the motion of the mechanical system. The applied PD input control vector $\mathbf{Q}_u$ that only controls the mechanical system is

$$\overline{\mathbf{Q}}_u = -\mathbf{K}_p(\mathbf{q}_r - \mathbf{q}_{rt}) - \mathbf{K}_d\dot{\mathbf{q}}_r, \tag{18}$$

where the $\mathbf{K}_p$ is the proportional gain vector, $\mathbf{K}_d$ is the derivative gain vector, and $\mathbf{q}_{rt}$ is the target position and the angle vector. The PD controller is chosen for this analysis to identify the influences of the cable in such a simple controller. The gains are set through a try-and-error operation through a preliminary study so that the influences of the cable appear significant. Table 1 shows the parameters of the numerical analysis.

Table 1. Parameters of numerical analysis.

Target position and angle $\mathbf{q}_{\text{rt}}$	$[2\ \ 0\ \ 0]^T$
Number of elements N	20
Gravitational acceleration g	9.81 (m/s^2)
Length of cable L_c	3 (m)
Cross-sectional area of cable A_c	0
Density of cable ρ_c	1500 (kg / m^3)
Young's modulus of cable E_c	1.0×10^6 (Pa)
Volume of rigid body V_r	$0.05\times0.05\times0.05$ (m^3)
Density of rigid body ρ_r	7870 (kg / m^3)
Friction coefficient μ	0.6

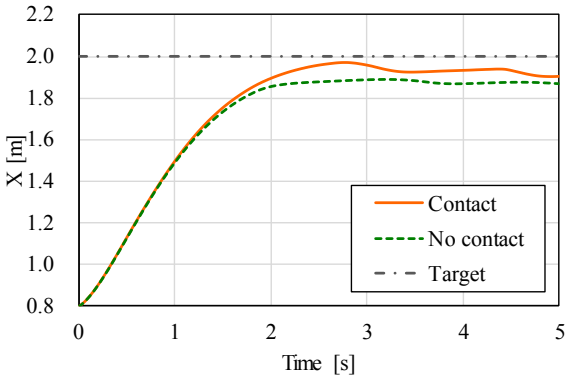

Fig. 6. Numerical analysis results: X coordinate of the connecting point of the cable and the rigid body.

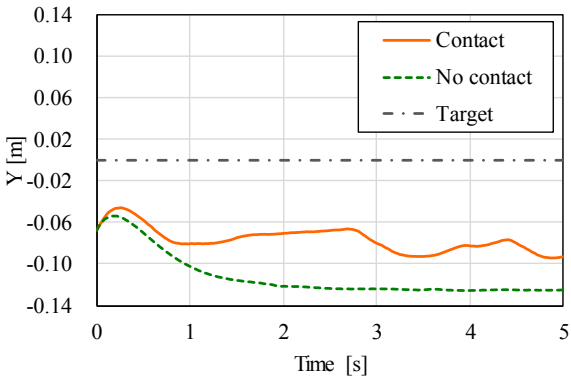

Fig. 7. Numerical analysis results: Y coordinate of the connecting point of the cable and the rigid body.

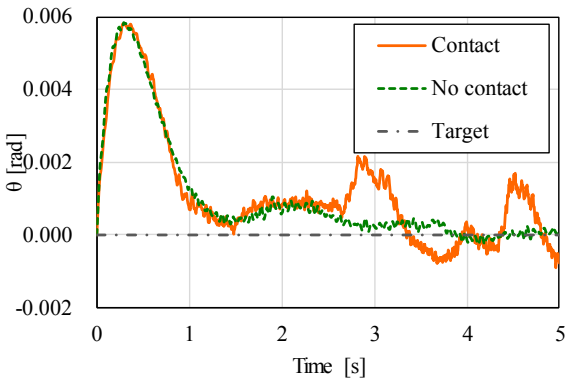

Fig. 8. Numerical analysis results: θ coordinate of the connecting point of the cable and the rigid body.

The numerical analysis shows two influences of the contact forces on the motion of the mechanical system. The mechanical system with the cable contacting the ground reached the target point closer than when it is free from touching any obstacles. It could be surmised that because of the normal force, the mechanical system had less drag on its movement. In contrast, the mechanical system with the cable contacting the ground was more unstable at the target position than the mechanical system with the cable without contact forces. When the cable length becomes shorter, the influence of its stiffness on the dynamics becomes significant, thus, the stiffness of the cable itself causes the vibration of the θ to occur. More simply put, the contact forces are working to disturb the mechanical system by causing the vibration. The results indicate that this proposed contact model is a qualitative model, showing vibration.

Note that this research focuses on a specific contacting situation when the cable contacts the ground between the two suspending points. The behaviour of the mechanical system differs between when there is contact force and when there is not. Hence, a new compensation system is needed for the mechanical system when connected to a cable which is making contact with the ground.

For higher accuracy of friction force distribution, an improved analysis model using the Gauss-Legendre quadrature is needed (Kerkkanen et al. 2006; Hasegawa et al., 2008; Lugris et al., 2010). When this proposed analysis model is put into practice, the frictional contact forces must be validated through experiments.

4. COMPENSATION SYSTEM FOR THE CABLE INFLUENCES

4.1 Coordinate transformation

The compensation is designed to break down the whole control system into the PD controller. The objective system is underactuated. Thus, the coordinates in the equation of motion, in which the control input can be directly applied, must be extracted by a coordinate transformation as the equations after (19) show.

$$\mathbf{M}\ddot{\mathbf{q}} = \mathbf{Q} \quad \Leftrightarrow \begin{bmatrix} \mathbf{M}_{11} & \mathbf{M}_{12} \\ \mathbf{M}_{21} & \mathbf{M}_{22} \end{bmatrix} \begin{bmatrix} \ddot{\mathbf{q}}_1 \\ \ddot{\mathbf{q}}_2 \end{bmatrix} = \begin{bmatrix} \mathbf{Q}_1 \\ \mathbf{Q}_2 \end{bmatrix}. \tag{19}$$

Firstly, the inertia matrix is transformed as

$$\mathbf{M} = \mathbf{T}_S{}^T \widetilde{\mathbf{M}} \mathbf{T}_S, \tag{20}$$

$$\mathbf{T}_S = \begin{bmatrix} \mathbf{I} & \mathbf{M}_{21}\mathbf{M}_{11}{}^{-1} \\ \mathbf{0} & \mathbf{I} \end{bmatrix}, \tag{21}$$

$$\widetilde{\mathbf{M}} = \begin{bmatrix} \mathbf{M}_{11} & \mathbf{0} \\ \mathbf{0} & \mathbf{M}_{22} - \mathbf{M}_{21}\mathbf{M}_{11}{}^{-1}\mathbf{M}_{12} \end{bmatrix}. \tag{22}$$

$\mathbf{q} = \mathbf{T}_S{}^{-1}\tilde{\mathbf{q}}$ is applied to (19) and yields

$$\mathbf{M}(\mathbf{T}_S{}^T\ddot{\tilde{\mathbf{q}}}) = \mathbf{Q}. \tag{23}$$

Multiplication by $\mathbf{T}_S{}^{-T}$ to both sides of (23) yields

$$(\mathbf{T}_S{}^{-T}\mathbf{M}\mathbf{T}_S{}^{-1})\ddot{\tilde{\mathbf{q}}} = \mathbf{T}_S{}^{-T}\mathbf{Q}. \tag{24}$$

Accordingly, (19) is coordinate transformed to (25) which is mathematically equal, denoting $\widetilde{\mathbf{M}} = \mathbf{T}_S{}^{-T}\mathbf{M}\mathbf{T}_S{}^{-1}$, $\widetilde{\mathbf{Q}} = \mathbf{T}_S{}^{-T}\mathbf{Q}$,

$$\widetilde{\mathbf{M}}\ddot{\tilde{\mathbf{q}}} = \widetilde{\mathbf{Q}}, \tag{25}$$

$$\ddot{\tilde{\mathbf{q}}} = \begin{bmatrix} \ddot{\mathbf{q}}_1 + \mathbf{M}_{11}{}^{-1}\mathbf{M}_{12}\ddot{\mathbf{q}}_2 \\ \ddot{\mathbf{q}}_2 \end{bmatrix}, \tag{26}$$

$$\tilde{\mathbf{Q}} = \begin{bmatrix} \mathbf{Q}_1 \\ \mathbf{Q}_2 + \mathbf{M}_{21}\mathbf{M}_{11}{}^{-1}\mathbf{Q}_1 \end{bmatrix}. \tag{27}$$

4.2 Control system

This section presents the control system for stabilizing the position and attitude of the mechanical system connected at the end of the cable. Yamamoto et al. (2019) proposed a compensation system using the Unscented Kalman Filter (UKF) for the cable influences of the gravitational force. This UKF is introduced to estimate the state of the cable and the mechanical system, which is required for the compensation system to achieve the control objective. As a result, it controlled the mechanical system with a cable efficiently. The equation of motion of the control objective in Newton-Euler form is

$$\begin{bmatrix} \mathbf{M}_{cc} & \mathbf{M}_{cr} \\ \mathbf{M}_{rc} & \mathbf{M}_{rr} \end{bmatrix} \begin{bmatrix} \ddot{\mathbf{q}}_c \\ \ddot{\mathbf{q}}_r \end{bmatrix} = \begin{bmatrix} \mathbf{Q}_c \\ \mathbf{Q}_r + \mathbf{Q}_u \end{bmatrix}, \tag{28}$$

where $\mathbf{M}_{cc}$, $\mathbf{M}_{cr}$, $\mathbf{M}_{rc}$, and $\mathbf{M}_{rr}$ each denotes the block element of inertia matrix for the cable and the rigid body, $\mathbf{q}_c$, $\mathbf{q}_r$ denotes the element of generalized coordinate vector for the cable and the rigid body, and $\mathbf{Q}_c$, $\mathbf{Q}_r$ denotes the element of external force vectors for the cable, the rigid body, and $\mathbf{Q}_u$ denotes the input vector. Taking note of the characteristic of ANCF where the inertia matrix is constant and applying the coordinate transformation shown in section 4.1 to the equation of motion (8), (28) is coordinate transformed into

$$\begin{bmatrix} \mathbf{M}_{cc} & \mathbf{0} \\ \mathbf{0} & \mathbf{M}_{rr} - \hat{\mathbf{M}} \end{bmatrix} \begin{bmatrix} \ddot{\mathbf{q}}_c + \ddot{\hat{\mathbf{q}}} \\ \ddot{\mathbf{q}}_r \end{bmatrix} = \begin{bmatrix} \mathbf{Q}_c \\ \hat{\mathbf{Q}} + \mathbf{Q}_r + \mathbf{Q}_u \end{bmatrix}, \tag{29}$$

noting $\hat{\mathbf{M}}$, $\hat{\mathbf{q}}$, and $\hat{\mathbf{Q}}$ are

$$\begin{aligned} \hat{\mathbf{M}} &= \mathbf{M}_{rc}\mathbf{M}_{cc}{}^{-1}\mathbf{M}_{cr}, \\ \hat{\mathbf{q}} &= \mathbf{M}_{cc}{}^{-1}\mathbf{M}_{cr}\ddot{\mathbf{q}}_r, \\ \hat{\mathbf{Q}} &= \mathbf{M}_{rc}\mathbf{M}_{cc}{}^{-1}\mathbf{Q}_c. \end{aligned} \tag{30}$$

Extracting the 2nd-row block element of (29), which is the equation related to the generalized coordinate vector of the rigid body, it can be transformed as

$$\left(\mathbf{M}_{rr} - \hat{\mathbf{M}}\right)\ddot{\mathbf{q}}_r = \hat{\mathbf{Q}} + \mathbf{Q}_r + \mathbf{Q}_u. \tag{31}$$

It is noticeable that $\hat{\mathbf{Q}}$ depends on state variables, especially, $\hat{\mathbf{Q}}$ can be calculated when the state variables are known. Here, the control input vector $\mathbf{Q}_u$ is

$$\mathbf{Q}_u = \bar{\mathbf{Q}}_u - \left(\hat{\mathbf{Q}} + \mathbf{Q}_r\right). \tag{32}$$

Substitution of (32) to the 2nd-row block element of (30) yields the equation of motion (33).

$$\left(\mathbf{M}_{rr} - \hat{\mathbf{M}}\right)\ddot{\mathbf{q}}_r = \bar{\mathbf{Q}}_u. \tag{33}$$

The inertia matrix $\mathbf{M}_{rr} - \hat{\mathbf{M}}$ is constant due to the characteristics of the ANCF. Regarding $\bar{\mathbf{Q}}_u$ as a new control input vector, (33) is the equation of motion of the rigid body with the control input applied. In other words, by applying $\bar{\mathbf{Q}}_u$ as (31), the proposed compensation system can compensate for the influence of the gravitational force and its stiffness on the cable $\hat{\mathbf{Q}}$ and the influences of the gravitational force on the rigid body $\mathbf{Q}_r$. The original control problem with the flexible structure is transformed to a rigid body control problem, thus, the mechanical system can be controlled. Therefore, knowing the appropriate control input vector $\bar{\mathbf{Q}}_u$ enables the mechanical system to stabilize the rigid body position and angle itself precisely. This compensation system should then allow the PD to control the mechanical system because the cable model was simplified, meaning it was redesigned to be rigid and not flexible. In this paper, the PD control input vector (34) is introduced.

$$\bar{\mathbf{Q}}_u = -\mathbf{K}_p\left(\mathbf{q}_r - \mathbf{q}_{rt}\right) - \mathbf{K}_d\dot{\mathbf{q}}_r. \tag{34}$$

The optimum gains are calculated using the linear quadratic regulator (LQR). The gains are chosen to minimize the performance index (35). The weights were determined through a preliminary study. However, the control accuracy could be changed by the weights (36) and (37).

$$J = \int_0^\infty (\mathbf{q}_r{}^T\mathbf{W}\mathbf{q}_r + \bar{\mathbf{Q}}_u{}^T\mathbf{R}\bar{\mathbf{Q}}_u)dt, \tag{35}$$

$$\mathbf{W} = \mathrm{diag}(w_1, w_2, w_3, w_4, w_5, w_6), \tag{36}$$

$$\mathbf{R} = \mathrm{diag}(r_1, r_2, r_3). \tag{37}$$

Using conventional FEMs, the inertia matrix for the cable depends on the variables. Thus, the inverse matrix of the block inertia matrices, that were needed in the transformation from (29) to (30), must be calculated at every computing step. In addition, the conventional FEMs use a greater number of elements than the ANCF, if the control input that compensates the influences of the cable yielded as (33). This is because a higher dimension of the inertia matrix is used in order to obtain a more accurate expression of the cable. Consequently, the conventional methods are not convincingly suitable for practical or analytical use because the calculation cost of the inverse matrix becomes extremely large. On the other hand, since the inertia matrix is constant using the ANCF, the inverse matrix calculation is necessary no more than once. Moreover, the size of the inertia matrix is smaller because fewer elements are required in the ANCF than the conventional FEMs for a flexible structure in which the deformation and the rotation are large. Therefore, the proposed method reduces the calculation cost compared to the conventional FEMs, and is, thus, a realistic method from the perspective of both practical and analytical use.

5. STATE ESTIMATION

The state estimation is necessary to apply (33) for precise control of the rigid body. Attaching many sensors to the cable to obtain all the state variables is extremely unrealistic and

difficult considering the practical use of UAVs. Hence, we propose to introduce the following state estimation method in addition to the proposed compensation system for the influences of the cable. In this paper, we assume the sensors are attached to obtain the position and the angle of the rigid body for estimating the state variables of the system including the cable using UKF.

The basic logic of the UKF is statistic approximation. To be more specific, the approximation of probability density function (probability distribution) as a normal distribution is used in the UKF. It is one of the statistical sampling methods that approximate probability distribution as the ensemble mean, by selecting a few sampling points that correspond with standard derivation called sigma points (σ point).

5.1 State Equation for Estimation

The state equation (38) is derived from (29) to apply the UKF state estimation to the proposed control method. The observation equation (39) is yielded (as follows) while it considers that the rigid body position and angle are known,

$$\frac{\mathrm{d}}{\mathrm{d}t}\begin{bmatrix}\mathbf{q}_c\\ \mathbf{q}_r\\ \dot{\mathbf{q}}_c\\ \dot{\mathbf{q}}_r\end{bmatrix}=\mathbf{A}\begin{bmatrix}\mathbf{q}_c\\ \mathbf{q}_r\\ \dot{\mathbf{q}}_c\\ \dot{\mathbf{q}}_r\end{bmatrix}+\mathbf{B}\mathbf{U}, \tag{38}$$

$$\mathbf{y}=\begin{bmatrix}\mathbf{0} & \mathbf{I} & \mathbf{0} & \mathbf{0}\end{bmatrix}\begin{bmatrix}\mathbf{q}_c\\ \mathbf{q}_r\\ \dot{\mathbf{q}}_c\\ \dot{\mathbf{q}}_r\end{bmatrix}, \tag{39}$$

noting **A**, **B**, and **U** are

$$\mathbf{A}=\begin{bmatrix}\mathbf{0} & \mathbf{I}\\ \widetilde{\mathbf{M}}^{-1}\widetilde{\mathbf{K}} & \mathbf{0}\end{bmatrix},\mathbf{B}=\begin{bmatrix}\mathbf{0}\\ \widetilde{\mathbf{M}}^{-1}\end{bmatrix},\mathbf{U}=\begin{bmatrix}\mathbf{Q}_{Ec}\\ \mathbf{Q}_r+\mathbf{Q}_u\end{bmatrix}. \tag{40}$$

Here, **M** and **K** are

$$\widetilde{\mathbf{M}}=\begin{bmatrix}\mathbf{M}_{cc} & \mathbf{M}_{cr}\\ \mathbf{M}_{rc} & \mathbf{M}_{rr}\end{bmatrix},\widetilde{\mathbf{K}}=\begin{bmatrix}\mathbf{K}_l+\mathbf{K}_t & \mathbf{0}\\ \mathbf{0} & \mathbf{0}\end{bmatrix}. \tag{41}$$

The $\mathbf{Q}_u$ is calculated using the estimated state value by UKF $\hat{\mathbf{q}}$ and applied to the control object as the control input.

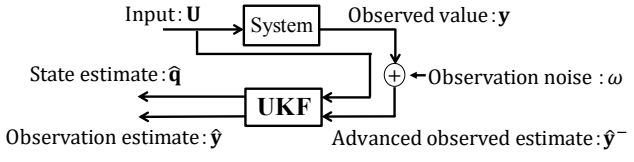

Fig. 9. The block diagram of state estimation using UKF.

5.2 State Estimation by UKF

This section considers a case when the state estimation initial value $\{\boldsymbol{y}(k)\}$ is modelled using the time-series, non-linear, state equation which is based on discrete-time, non-linear, state-space expressions:

$$\boldsymbol{q}(k-1)=\boldsymbol{a}(\boldsymbol{q}(k))+\boldsymbol{b}\upsilon(k), \tag{42}$$

$$\boldsymbol{y}(k)=\boldsymbol{c}(\boldsymbol{q}(k))+\boldsymbol{d}\omega(k). \tag{43}$$

Here, $\boldsymbol{a}$ and $\boldsymbol{c}$ denote non-linear functions $\boldsymbol{q}(k)$ that take vector values, and k denotes the time-series ordinal number. The system noise is denoted as $\upsilon(k)$, observation noise is denoted as $\omega(k)$, which are normal white noises when the mean value 0, the variance $\sigma_v^2(k)$, the mean value 0, and the variance $\sigma_\omega^2(k)$ are independent of each other.

The state estimation is performed using the UKF algorithm targeted on filtering the time-series $y(k)$, which is expressed by above non-linear state equations. At first, initial values of state estimate and covariance matrix are set as follows:

$$\hat{\boldsymbol{q}}(0)=E[q(0)]=\boldsymbol{q}_{\boldsymbol{0}}, \tag{44}$$

$$\mathbf{P}(0)=E[(q(0)-E[q(0)])(q(0)-E[q(0)])^T]=\boldsymbol{\Sigma}_{\boldsymbol{0}}, \tag{45}$$

Furthermore, the variance of the system noise $\sigma_\upsilon^2(k)$ and the variance of the observation noise $\sigma_\omega^2(k)$ is determined. Then, the sigma point and the predicting step are calculated for each step $k=1,2,\ldots,N$. The $2n+1$ sigma points are calculated from the covariance matrix $\mathbf{P}(k-1)$ and the state estimate value $\hat{\mathbf{q}}(k-1)$ following (46), (47), and (48).

$$\boldsymbol{Q}_0(k-1)=\hat{\boldsymbol{q}}(k-1), \tag{46}$$

$$\boldsymbol{Q}_i(k-1)=\hat{\boldsymbol{q}}(k-1)+\sqrt{n+\kappa}(\sqrt{\mathbf{P}(k-1)})_i, i=1,2,\cdots,n, \tag{47}$$

$$\boldsymbol{Q}_{n+i}(k-1)=\hat{\boldsymbol{q}}(k-1)-\sqrt{n+\kappa}(\sqrt{\mathbf{P}(k-1)})_i, i=1,2,\cdots,n. \tag{48}$$

The sigma points are renewed as (49) and the preliminary state variable $\hat{\mathbf{q}}^-(k)$ and preliminary error covariance matrix $\mathbf{P}^-(k)$ are yielded from the renewed sigma points as (50) and (51)

$$\boldsymbol{Q}_i^-(k)=\boldsymbol{a}(\boldsymbol{Q}_i(k-1)), i=0,1,2,\cdots,2n, \tag{49}$$

$$\hat{\boldsymbol{q}}^-(k)=\sum_{i=0}^{2n}\omega_i\boldsymbol{Q}_i^-(k), \tag{50}$$

$$\hat{\boldsymbol{q}}^-(k)=\sum_{i=0}^{2n}\omega_i\{\boldsymbol{Q}_i^-(k)-\hat{\boldsymbol{q}}^-(k)\}\{\boldsymbol{Q}_i^-(k)-\hat{\boldsymbol{q}}^-(k)\}^T+{\sigma_\upsilon}^2\boldsymbol{b}\boldsymbol{b}^T, \tag{51}$$

where, the weights are

$$\omega_0=\frac{\kappa}{n+\kappa}, \tag{52}$$

$$\omega_i=\frac{\kappa}{2(n+\kappa)}, i=1,2,\cdots,2n. \tag{53}$$

The sigma point is recalculated from the preliminary state variable $\hat{\boldsymbol{q}}^-(k)$ and the preliminary error covariance matrix $\mathbf{P}^-(k)$ as

$$\boldsymbol{Q}_0^-(k)=\hat{\boldsymbol{q}}^-(k), \tag{54}$$

$$\boldsymbol{Q}_i^-(k)=\hat{\boldsymbol{q}}^-(k)+\sqrt{n+\kappa}\left(\sqrt{\mathbf{P}^-(k)}\right)_i, i=1,2,\cdots,n, \tag{55}$$

$$\boldsymbol{Q}_{n+i}^-(k)=\hat{\boldsymbol{q}}^-(k)-\sqrt{n+\kappa}\left(\sqrt{\mathbf{P}^-(k)}\right)_i, i=1,2,\cdots,n. \tag{56}$$

After the recalculation of the sigma points, (57) shows the renewal of the sigma points. The preliminary output estimate $\hat{\boldsymbol{y}}^-(k)$, the preliminary output error covariance matrix $\mathbf{P}_{yy}^-(k)$, and the preliminary state/output error covariance matrix $\mathbf{P}_{qy}^-(k)$ are calculated from the renewed sigma points.

$$\boldsymbol{Y}_i^-(k)=\boldsymbol{c}(\boldsymbol{Q}_i^-(k)), i=0,1,2,\cdots,2n, \tag{57}$$

$$\hat{\boldsymbol{y}}^-(k)=\sum_{i=0}^{2n}\omega_i\boldsymbol{Y}_i^-(k), \tag{58}$$

$$\mathbf{P}_{yy}^-(k)=\sum_{i=0}^{2n}\omega_i\left\{\boldsymbol{Y}_i^-(k)-\hat{\boldsymbol{y}}^-(k)\right\}\left\{\boldsymbol{Y}_i^-(k)-\hat{\boldsymbol{y}}^-(k)\right\}^T+\sigma_\omega{}^2\boldsymbol{d}\boldsymbol{d}^T, \tag{59}$$

$$\mathbf{P}_{qy}^-(k)=\sum_{i=0}^{2n}\omega_i\left\{\boldsymbol{Q}_i^-(k)-\hat{\boldsymbol{q}}^-(k)\right\}\left\{\boldsymbol{Y}_i^-(k)-\hat{\boldsymbol{y}}^-(k)\right\}^T. \tag{60}$$

Using the above, the Kalman gain $\mathbf{g}(k)$ is

$$\boldsymbol{g}(k)=\frac{\mathbf{P}^-{}_{qy}(k)}{\mathbf{P}^-{}_{yy}(k)}. \tag{61}$$

The state estimate $\hat{\boldsymbol{q}}(k)$ and the covariance matrix $\mathbf{P}(k)$ are derived as

$$\hat{\boldsymbol{q}}(k)=\hat{\boldsymbol{q}}^-(k)+\boldsymbol{g}(k)\left(\boldsymbol{y}(k)-\hat{\boldsymbol{y}}^-(k)\right). \tag{62}$$

$$\mathbf{P}(k)=\mathbf{P}^-(k)-\boldsymbol{g}(k)\left(\mathbf{P}^-{}_{qy}(k)\right)^T. \tag{63}$$

6. EVALUATION OF THE COMPENSATION SYSTEM AND STATE ESTIMATION

This section presents the numerical analysis with the proposed compensation system with the proposed state estimation applied. As the initial state, the rigid body is at the origin of the coordinates and the cable is in a slack state. The PD controller with the compensation system for the rigid body is

$$\overline{\mathbf{Q}}_u=-\mathbf{K}_p(\mathbf{q}_r-\mathbf{q}_{rt})-\mathbf{K}_d\dot{\mathbf{q}}_r. \tag{64}$$

Table 2 shows the parameters of the numerical analysis.

Table 2. Parameters of numerical analysis.

Target position and angle $\mathbf{q}_{rt}$	$[2 \quad 0 \quad 0]^T$
Number of elements N	20
Gravitational acceleration g	9.81 (m/s^2)
Length of cable L_c	3 (m)
Cross-sectional area of cable A_c	0.005×0.005 (m^2)
Density of cable ρ_c	1500 (kg / m^3)
Young's modulus of cable E_c	1.0×10^6 (Pa)
Volume of rigid body V_r	$0.05\times0.05\times0.05$ (m^3)
Density of rigid body ρ_r	7870 (kg / m^3)
Friction coefficient μ	0.6

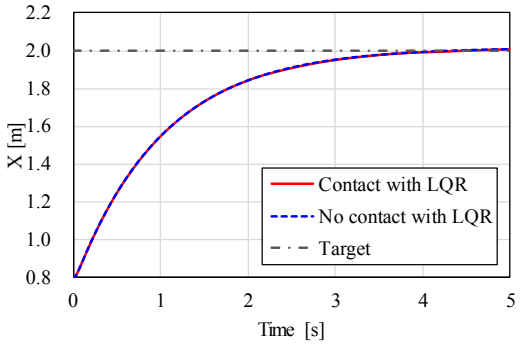

Fig. 10. Numerical analysis results: X coordinate of the connecting point of the cable and the rigid body.

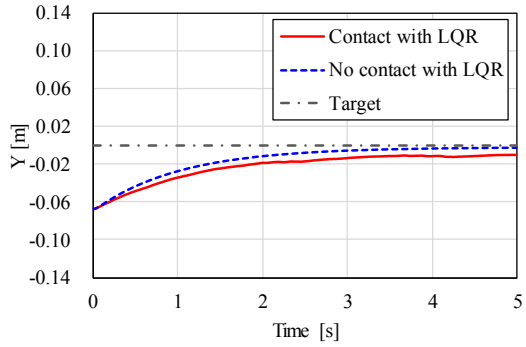

Fig. 11. Numerical analysis results: Y coordinate of the connecting point of the cable and the rigid body.

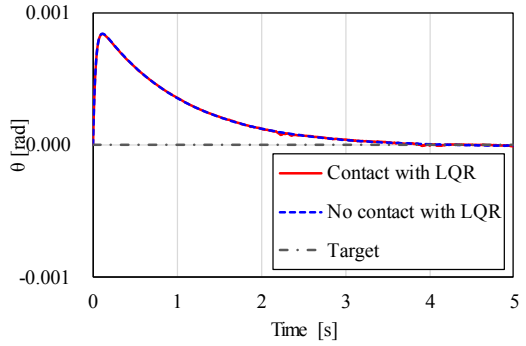

Fig. 12. Numerical analysis results: θ coordinate of the connecting point of the cable and the rigid body.

The numerical analysis shows that the proposed compensation system using the state estimation controls the rigid body with almost no error in the X axis direction and the θ axis direction. It also indicates that it stabilizes the rigid body at a certain point in the Y axis direction, yet there is an error of 10 cm. It can be said that the rigid body is stabilized by the compensation system. However, to compensate for the vertical error, the compensation system must be improved. Moreover, depending on the cable contacting model, the forces applied to the cable could differ, which may have a more major and negative effect on the compensation system. It must be noted that the present compensation system is only valid in limited conditions.

For the same reason that the PD controller design process using the LQR was not modified for the ground-contacting model, the present compensation system might show an

adequate control performance. As for future works, the compensation system must be improved to meet various operational situations when the forces on a UAV might differ from that of our experiment. In such a real-life case, these forces might have a major negative effect on its mechanical system's behaviour.

7. CONCLUSION

This paper presented an analytical evaluation for the control system of a mechanical system with a cable contacting the ground utilizing a two-dimensional model. In addition, this model derived the contact force by using the catenary curve for the attached cable to the mechanical system. The behaviour of the mechanical system using this proposed model was evaluated by a numerical analysis. The numerical analysis results showed the influences of the cable contact friction force on the mechanical system's motion. The influences of the cable contact help the mechanical system reach the target position in the horizontal and vertical direction, but they also cause unwanted vibration. The compensation system was designed to be broken down into a simple PD controller. The numerical analysis results showed that one of the influences of the cable contact friction force on the mechanical system's motion, an error in the vertical direction, remained while using the proposed control system. However, the analysis proved that the proposed control system, PD control input based on state estimation using UKF, manages to stabilize the mechanical system.

In future work, in order to achieve a higher accuracy of friction force distribution in the analysis model, the Gauss-Legendre quadrature will be used. Then, it will be validated through experiments. As for the compensation system, the PD controller design will be modified to meet an objective situation and improved for situations when the forces in the analysis model vary. Finally, the experimental verification for the proposed control system will be presented.

ACKNOWLEDGEMENT

We would like to express our thanks and gratitude to Associate Professor Charles E. Robertson for the supportive guidance when preparing this manuscript. This work was supported by JSPS KAKENHI Grant Number 19K04277.

REFERENCES

Berzeri, M., and Shabana, A. A. (2000). Development of simple models for the elastic forces in the absolute nodal co-ordinate formulation. *Journal of Sound and Vibration*, 235 (4), pp.539-565.

Ciampa, E., Vito, L. D., and Pecce, M. R. (2019). Practical issues on the use of drones for construction inspections. Journal of Physics: Conference Series, 1249 (1), 012016.

Hasegawa, T., Yoshida, T., and Hosoda, Y. (2008). *Mathematics for Engineering, Numerical Calculation for Engineering (published in Japanese)*, pp.161-165. SUURIKOUGAKUSHA-SHA, Tokyo, Japan.

Imadu, A., Noguchi, H., and Kawai, T. (2016). Optimum cable length for helicopter with cable to ground station. *Transactions of the Society of Instrument and Control Engineers*, 52 (4), pp. 220-227.

Kerkkanen, K., Garcia-Vallejo, D., and Mikkola, A. M. (2006). Modeling of belt-drives using a large deformation finite element formulation. *Nonlinear Dynamics*, 43 (3), pp.239-256.

Koyanagi, E. (2016). Response robot -Fukushima Daiichi Nuclear Power Plants using mobile rescue robot-. *Journal of the Robotics Society of Japan*, 34 (10), pp. 671-675.

Lugris, U., Escalona, J. L., Dopico, D., and Cuadrado, J. (2010). Efficient and accurate simulation of the cable-pulley interaction in weight-lifting machines. *The 1st Joint International Conference on Multibody System Dynamics*, Lappeenranta, Finland.

Michael, N., Shen, S., Mohta, K., Mulgaonkar, Y., Kumar, V., Nagatani, K., Okada, Y., Kiribayashi, S., Otake, K., Yoshida, K., Ohno, K., Takeuchi, E., and Tadokoro, S. (2012). Collaborative mapping of an earthquake-damaged building via ground and aerial robots. *Journal of Field Robotics*, 29 (5), pp. 832-841.

Ohno, K., Tadokoro, S., Michael, N., and Kruijff, G. J. M. (2015). *Special Issue on Disaster Response Robotics (2), Advanced Robotics*, 29 (3), pp. 147.

Rubio, J. J. (2018). Robust feedback linearization for nonlinear processes control. *ISA Transactions*, 74, pp. 155-164.

Rubio, J. J., Ochoa, G., Mujica-Vargas, D., Garicia, E., Balcazar, R., Elias, I., Curz, D. R., Juarez, C. F., Aguilar, A., and Novoa, J. F. (2019). Structure regulator for perturbations attenuation in a quadrotor. *IEEE Access*, 7, pp.138244-138252.

Yamamoto, T., Sugawara, Y., and Sakama, S. (2019). A study on motion analysis and control of mechanical systems connected by a cable. *Transactions of the JSME (in Japanese)*, 85 (875), pp. 18-00455.